

We are IntechOpen, the world's leading publisher of Open Access books Built by scientists, for scientists

4,800

Open access books available

122,000

International authors and editors

135M

Downloads

Our authors are among the

154

Countries delivered to

TOP 1%

most cited scientists

12.2%

Contributors from top 500 universities



WEB OF SCIENCE™

Selection of our books indexed in the Book Citation Index
in Web of Science™ Core Collection (BKCI)

Interested in publishing with us?
Contact book.department@intechopen.com

Numbers displayed above are based on latest data collected.
For more information visit www.intechopen.com



Studying the Flow Dynamics Within Endografts in Abdominal Aortic Aneurysms

Efstratios Georgakarakos, Antonios Xenakis, George S. Georgiadis, Konstantinos C. Kapoulas, Evangelos Nikolopoulos and Miltos Lazarides

Additional information is available at the end of the chapter

<http://dx.doi.org/10.5772/46034>

1. Introduction

Endovascular Treatment (EVAR) is considered the treatment of choice for the majority of Abdominal Aortic Aneurysms (AAA) nowadays, since it demonstrates improved perioperative morbidity and aneurysm-related mortality, comparing to conventional open repair. However, despite the initial technical success and early discharge of the patient, this technique is amenable to early and late complications, the most important of which are the endoleaks (ie. recurrence of blood flow detection within the aneurysm sac) accompanied sometimes with variable degrees of intrasac pressurization (Georgakarakos et al, 2012a). Furthermore, the hemodynamic changes that the endograft sustains during the follow-up period make it prone to positional changes with subsequent risk for endograft migration and loss of sealing between the endograft and either the aneurysm neck or the iliac fixation sites.

Computer-enhanced geometric modeling and Finite Volume Analysis have been used to study the biomechanical behavior of the aortic aneurysms before and after the insertion of the endograft device (Georgakarakos et al, 2012b). Numerical modeling of endovascular-treated AAA is used to determine the stresses and forces developed on AAA sac and stent-graft materials in-vivo, estimating hemodynamic parameters, such as the pressure and stress distribution over the main body, the bifurcation, the limbs of a stent-graft or the drag and displacement forces predisposing to graft migration. Consequently, the study of flow dynamics within aortic endografts holds a fundamental role in the delineation of the endograft behavior under pulsatile flow, providing useful information for developing and modifying the endograft design and surgical techniques. This chapter discusses the aforementioned changes, by using three-dimensional (3D) reconstructed endograft model.

2. Reconstruction of the AAA endograft model

Finite Volume Analysis technique has a crucial role in the computational research of hemodynamic systems, utilizing small subsections (elements) of 3-dimensional structures created by segmentation and meshing. By solving Navier-Stokes equations for all finite volumes of the model, Computational flow dynamics (CFD) techniques utilize numerical methods and algorithms to analyze problems that involve fluid flows. Furthermore, Fluid Structure Interaction (FSI) methods combine fluid and structural equations, solved either simultaneously or separately (partitioned approach), in order to determine the flow fields and solid body stresses on a deformable model. Most researchers acquire information on the 3D AAA realistic, complex geometry using patient-specific DICOM data derived from high-resolution spiral CT or MR angiography (Georgakarakos et al, 2012b).

Our study group used a reconstructed 3D model of a AAA endograft using commercially available appropriate, validated software (MIMICS 13.0, Materialise NV, Leuven, Belgium), based on the DICOM images derived from contrast-enhanced high-resolution computed tomography. The computational model (**Figure1**) includes the aortic neck proximal to the endograft and the iliac arteries distal to the endograft limbs. A validated Finite Volume analysis software ANSYS v 12.1 (Ansys Inc., Canonsburg, PA, USA) was used for Computational Fluid Dynamics (CFD). The velocity and pressure waveforms during a period of 1.2 s as previously described in a one-dimensional fluid-dynamics model for the abdominal aorta (Olufsen et al, 2000 and Li et al, 2005) were used for both models as inlet and outlet boundary conditions. Blood was assumed to be non-Newtonian fluid, according to the Carreau-Yasuda model, with a density of 1050 kg/m^3 .

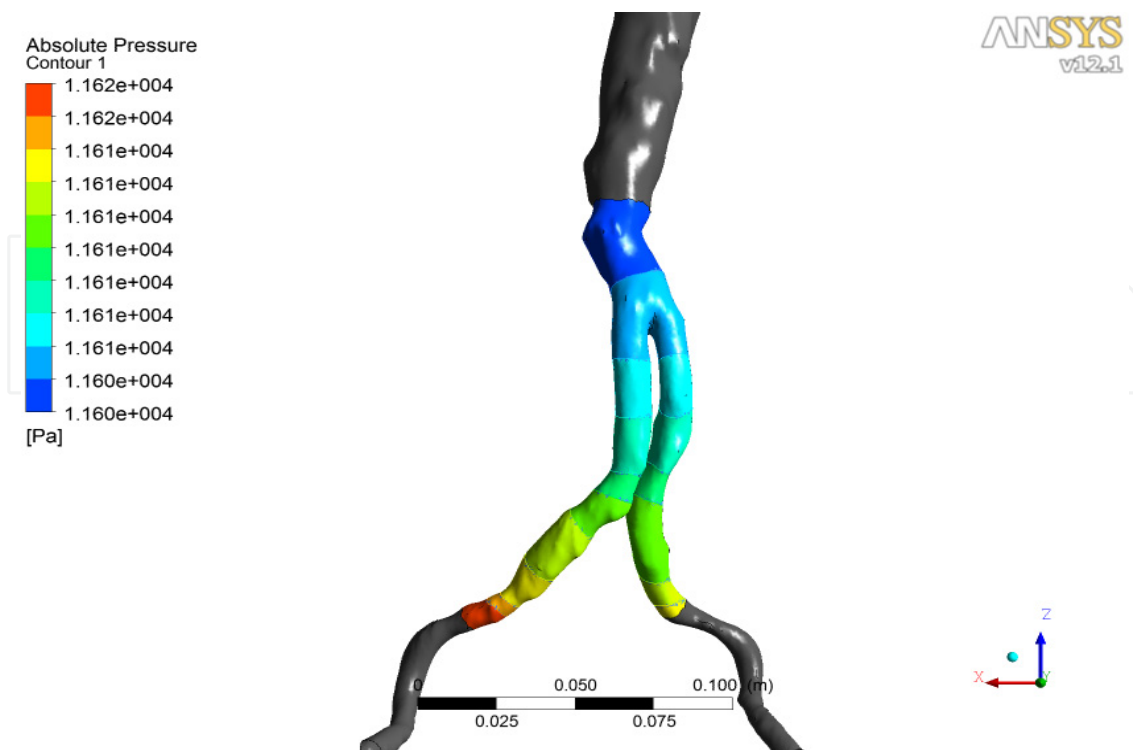


Figure 1. Reconstructed images of the aortic endograft using purpose-developed software.

Accordingly, the velocity streamlines and the pressure distribution were calculated over the entire surface of the endograft and are demonstrated in 6 distinct time-phases through the cardiac cycle (**Figure 2**). For study reasons, the cardiac cycle was divided in six distinct phases, namely the late diastole (t_1), the accelerating systolic phase (t_2), the peak systolic phase (t_3), the late deceleration (t_4), the end-systolic (t_5) and the early diastolic phase (t_6).

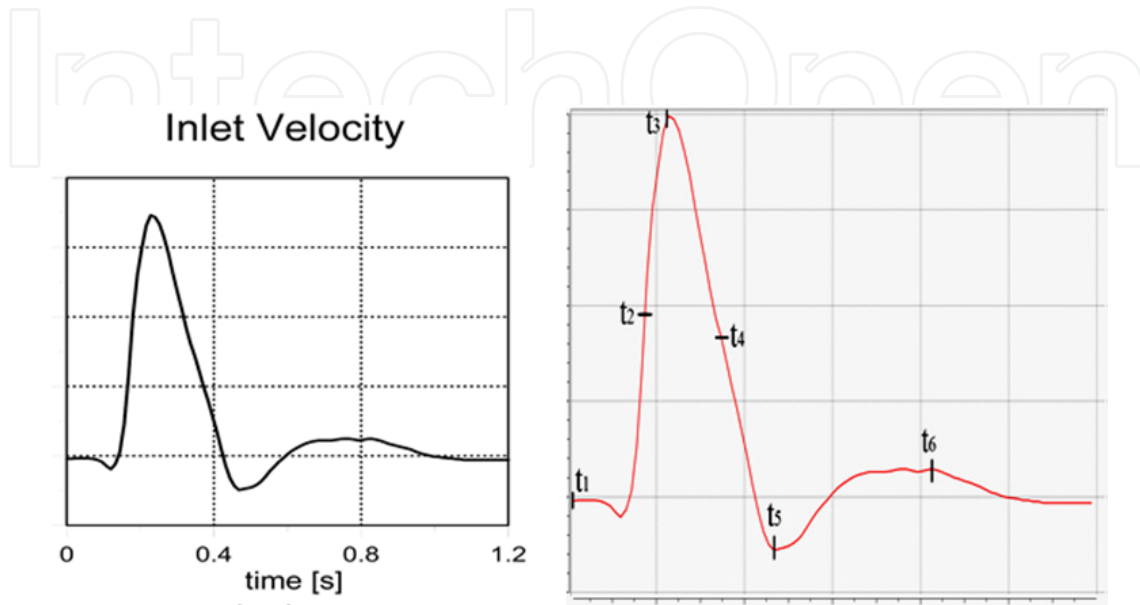


Figure 2. Plot of the flow waveform used for the calculations in our endograft model (left panel). Six distinct phases are depicted in each cardiac cycle. t_1 depicts the late diastole, t_2 the accelerating phase, t_3 represents the peak systolic phase, t_4 the late deceleration, t_5 depicts the end-systole and t_6 the early diastolic phase (right panel).

3. Changes in flow patterns and pressure distribution

Figures 3-8 depict the flow patterns in the endograft throughout the cardiac cycle. A flow disturbance is seen near the inlet zone (panel top-left) during the late diastole, t_1 (Figure 3). The flow pattern is normalized during the entire systolic phase, ie. t_2 to t_4 (Figures 4-6) and exhibits disturbance again, from the the end-systole t_5 early diastole t_6 (Figures 7,8). Interestingly, there is disturbed flow in the iliac limb unilaterally (left) during the decelerating systolic phase (Figure 6), whereas the irregular flow is also transmitted in the contralateral (right) iliac limb, during the next time-step (end-systolic phase, t_5 , Figure 7).

	t_1	t_2	t_3	t_4	t_5	t_6
Pressure values (mmHg)						
Max	87	167	147	120	104	97
Min	87	136	136	115	102	96

Table 1. Maximum and minimum values of pressure in the endograft surface, for the different phases of the cardiac cycle. Excessively high values of pressure due to alteration in the iliac limbs geometry were excluded (outlier values).

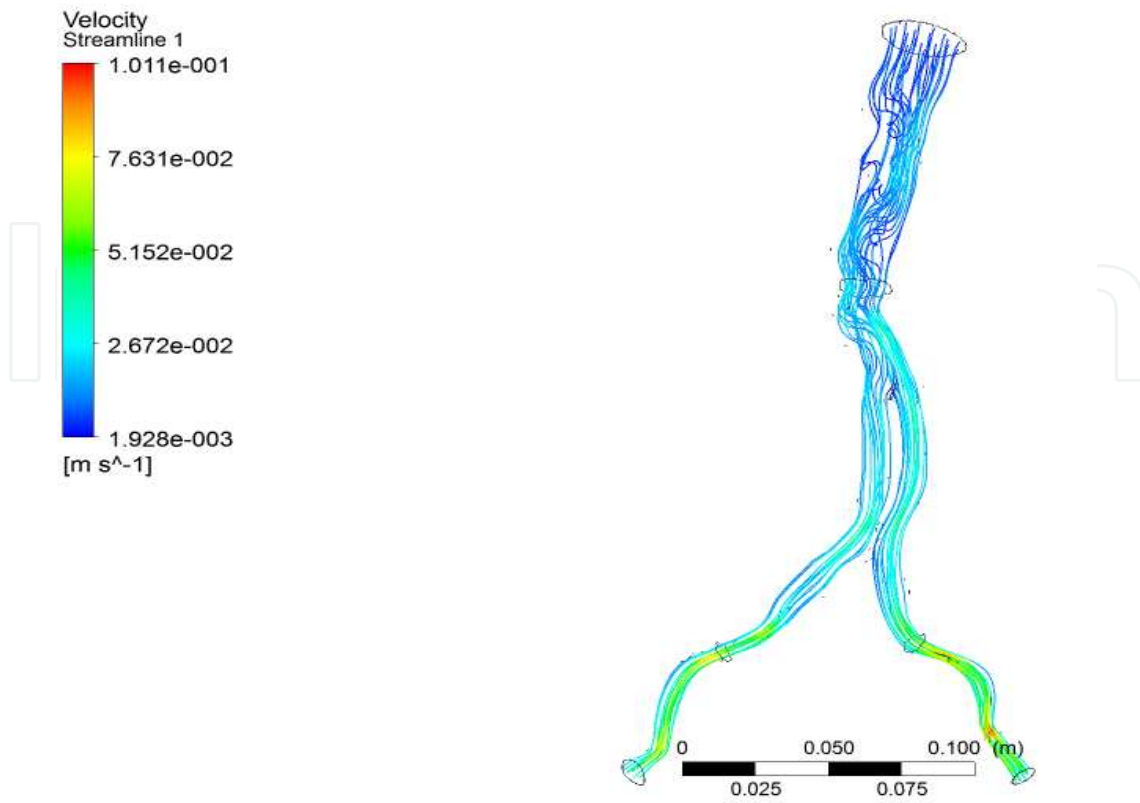


Figure 3. The velocity streamlines, as demonstrated for the late diastolic phase (t₁).

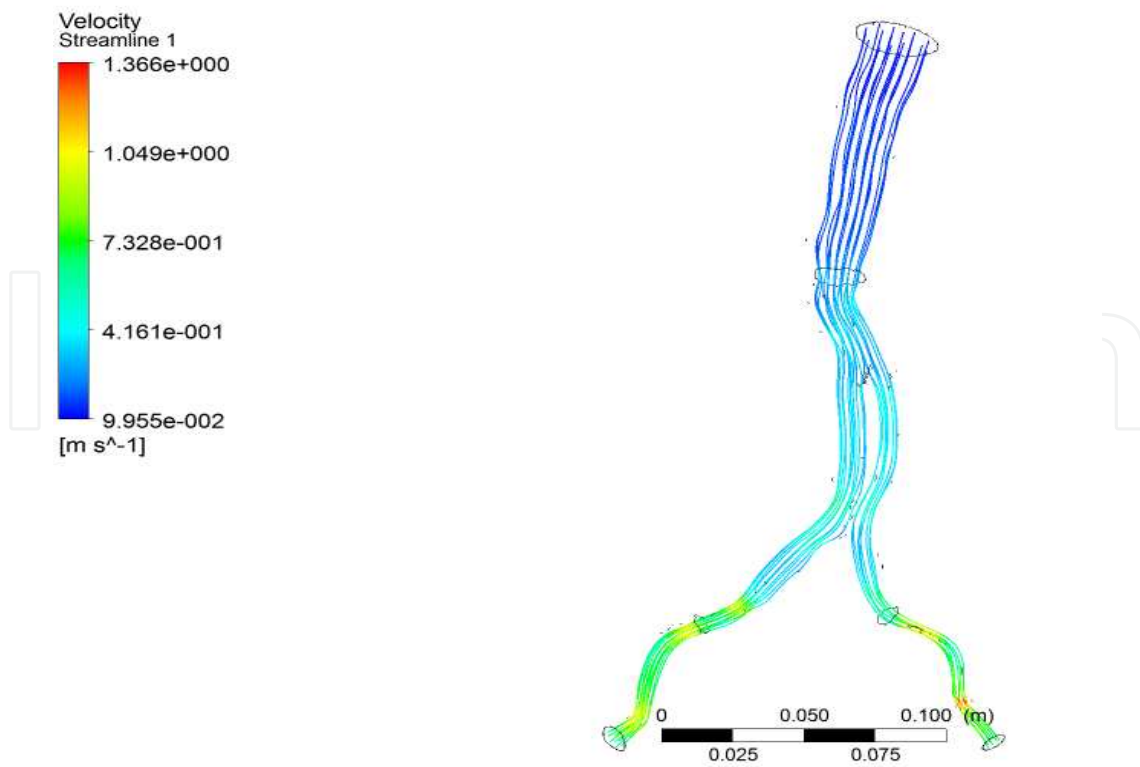


Figure 4. The velocity streamlines, as demonstrated for the accelerating systolic phase (t₂).

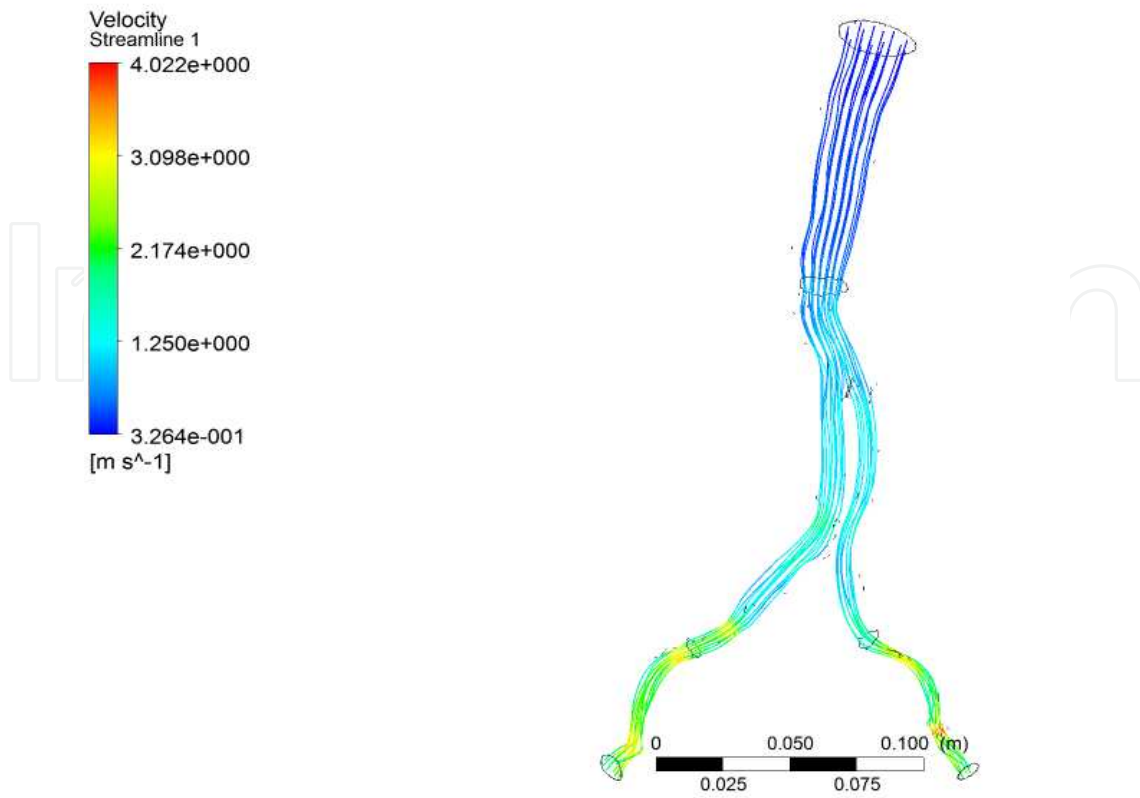


Figure 5. The velocity streamlines, as demonstrated for the peak systolic phase (t_3).

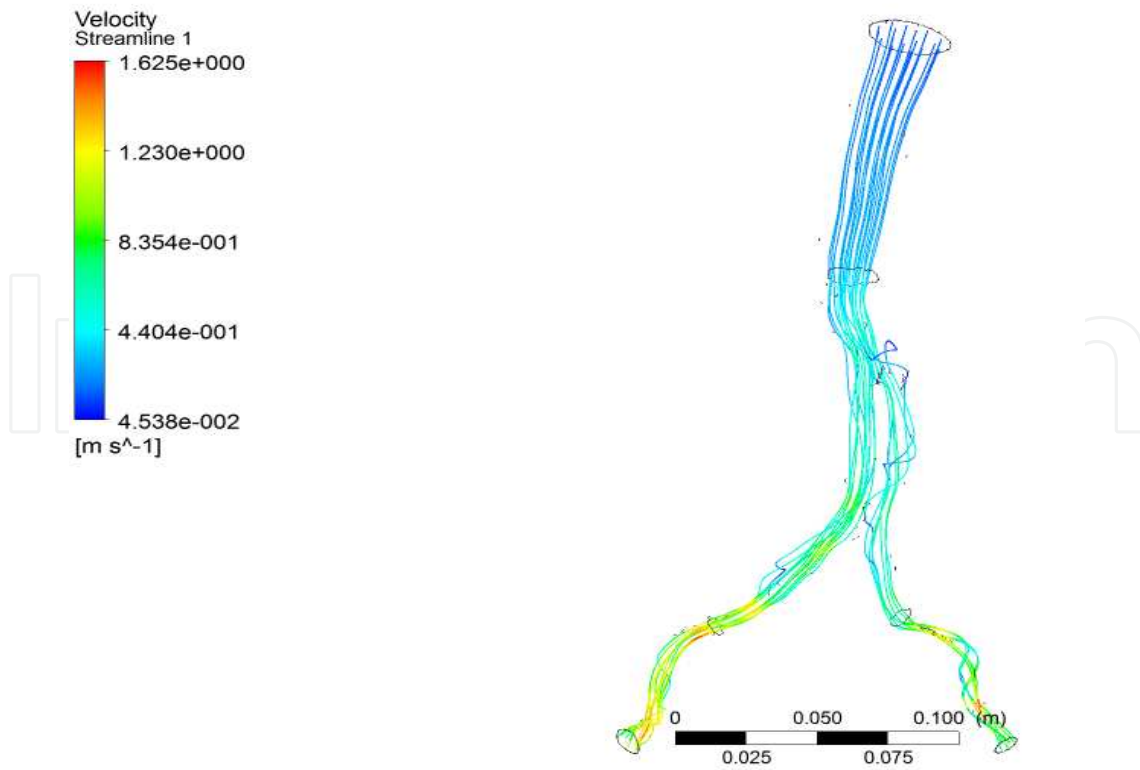


Figure 6. The velocity streamlines, as demonstrated for the decelerating systolic phase (t_4).

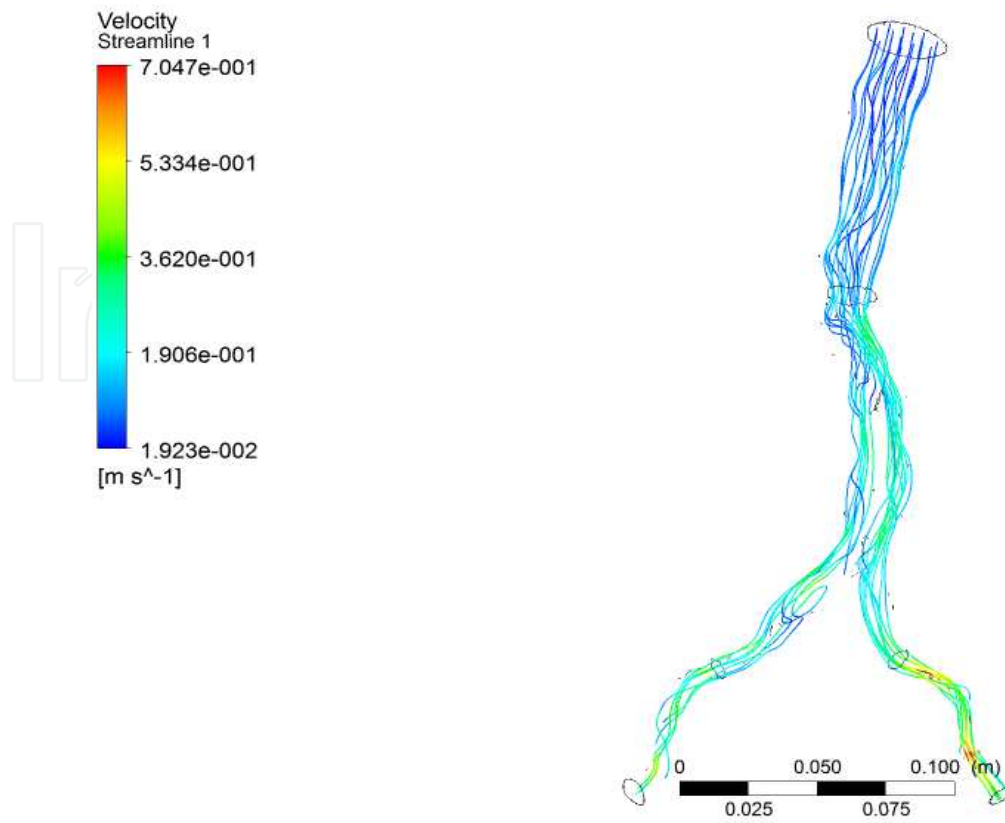


Figure 7. The velocity streamlines, as demonstrated for the end-systolic phase (t_5).

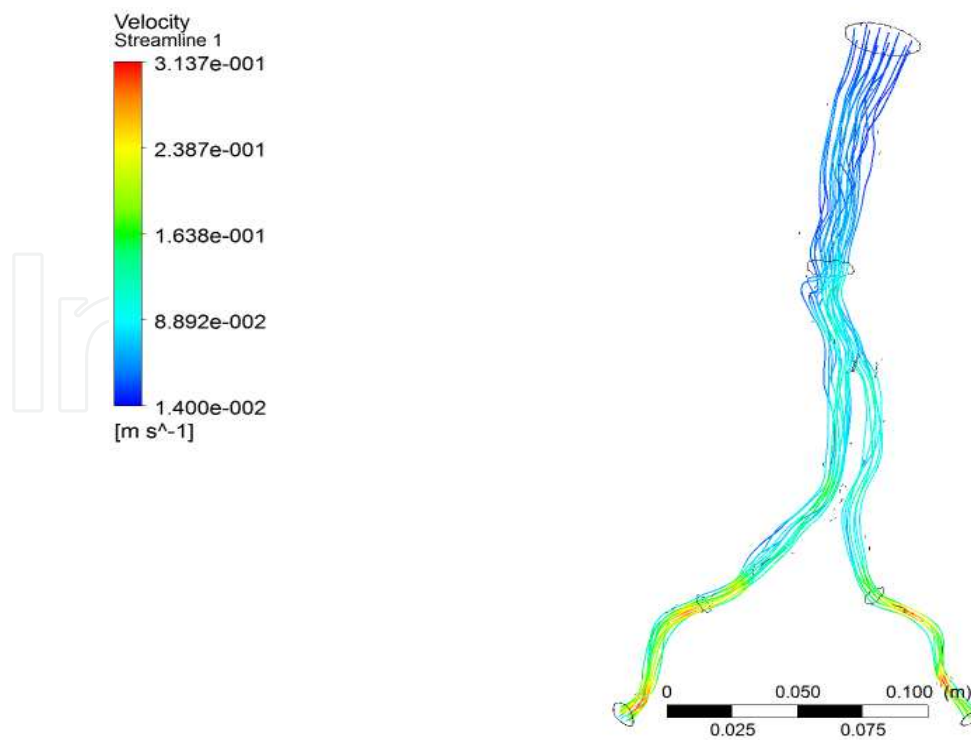


Figure 8. The velocity streamlines, as demonstrated for the early diastolic phase (t_6).

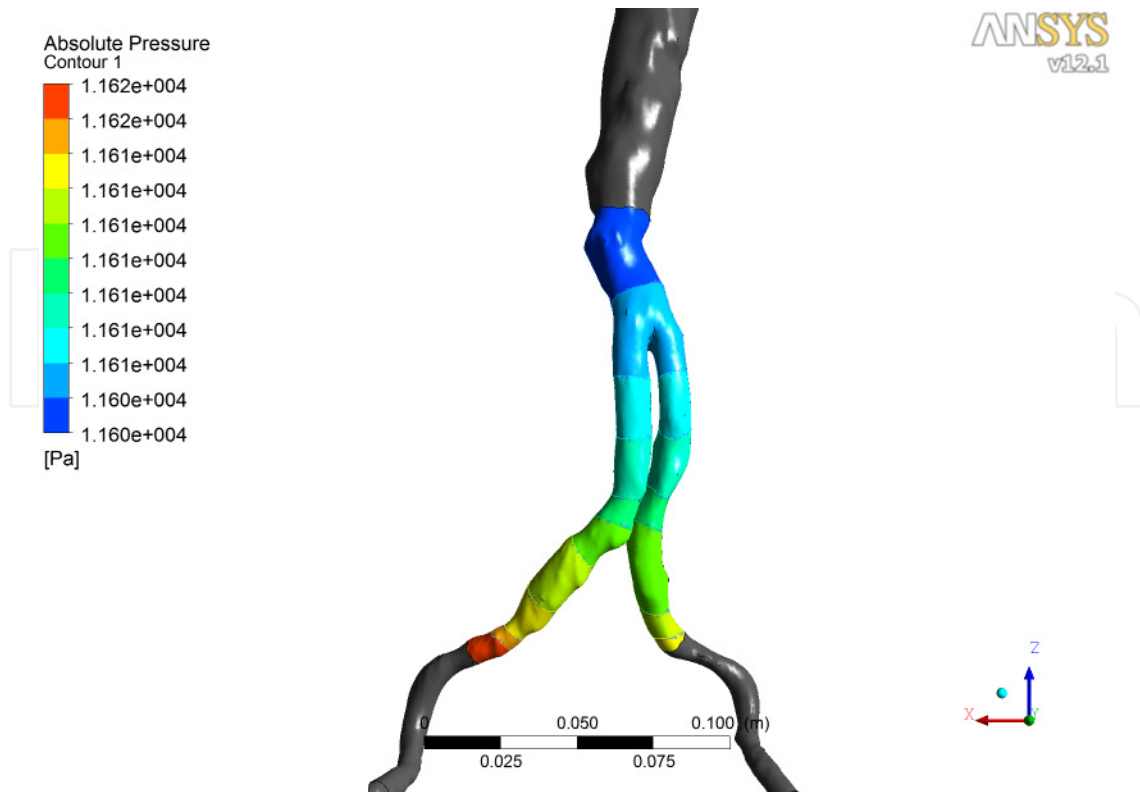


Figure 9. The distribution of pressures across the endograft, as demonstrated for the late diastolic phase (t_1).

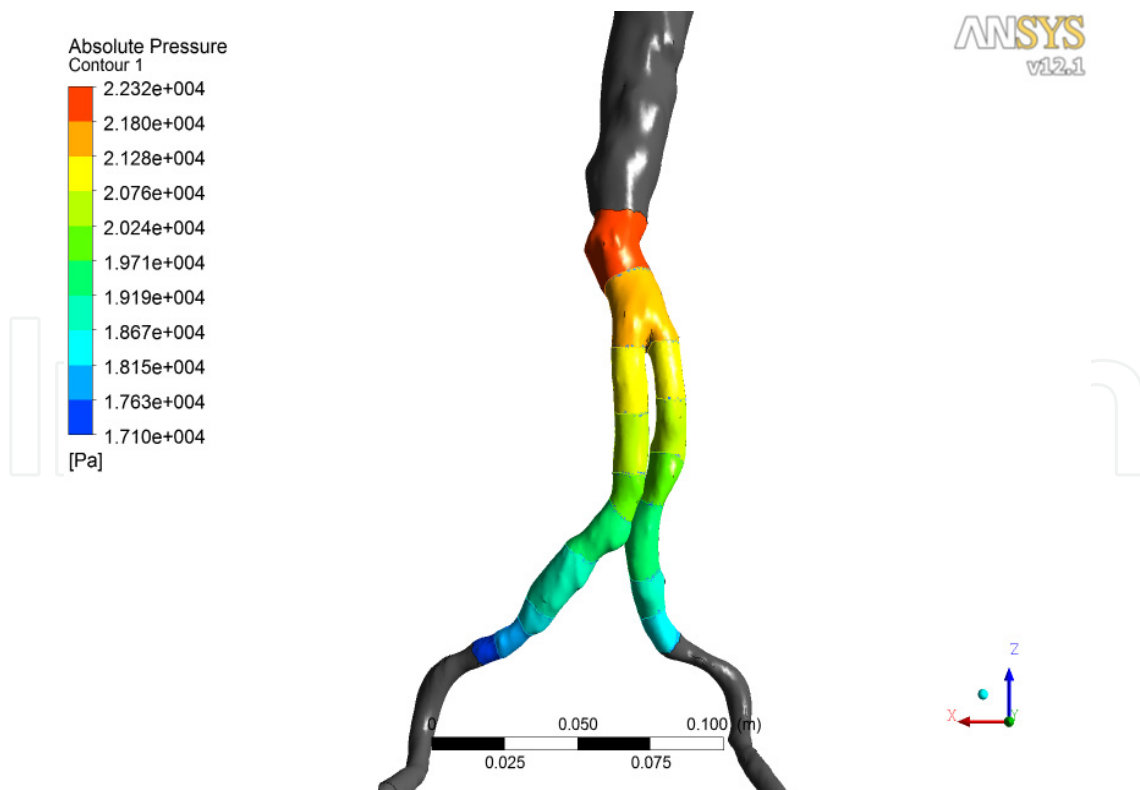


Figure 10. The distribution of pressures across the endograft, as demonstrated for the accelerating systolic phase (t_2).

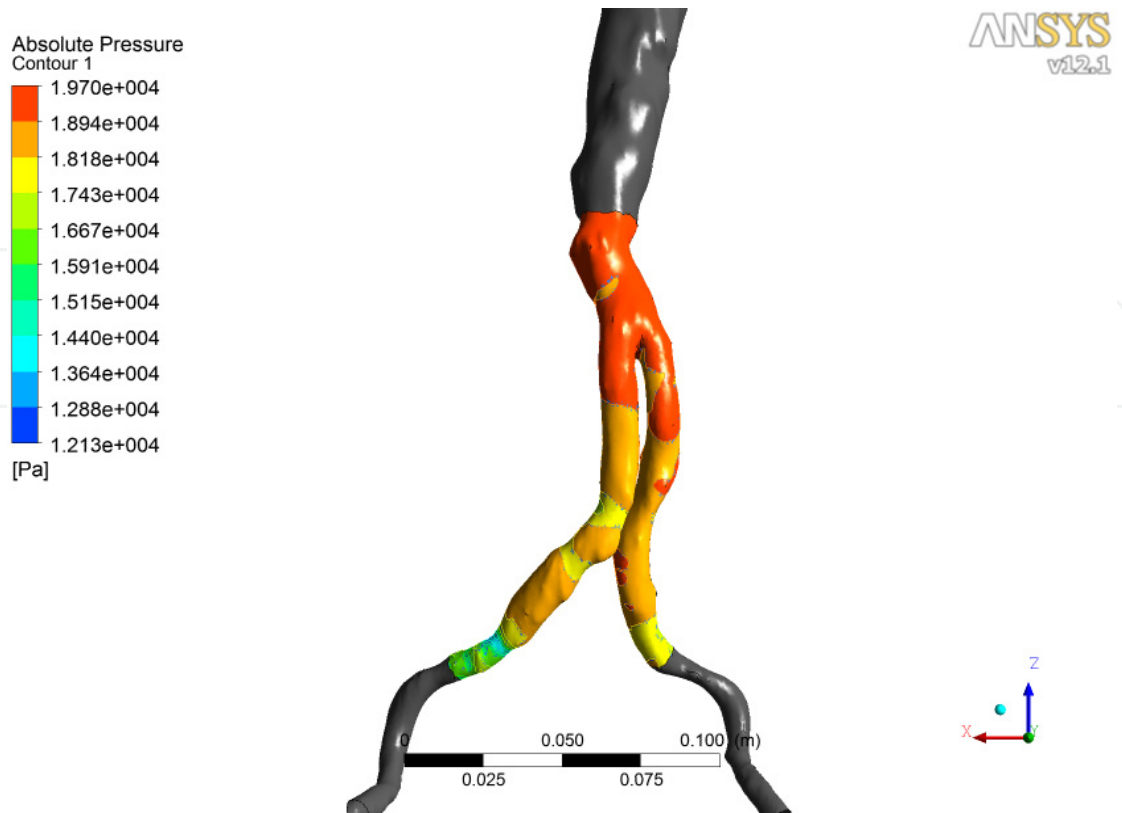


Figure 11. The distribution of pressures across the endograft, as demonstrated for the peak systolic phase (t_3).

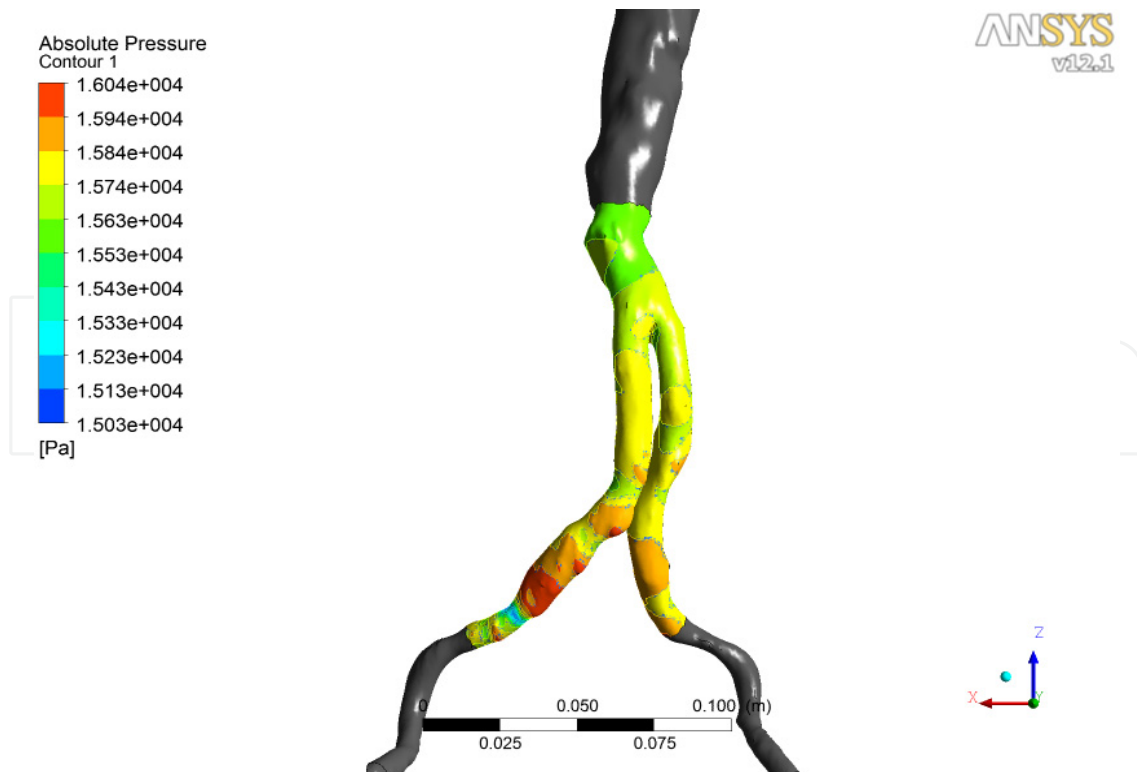
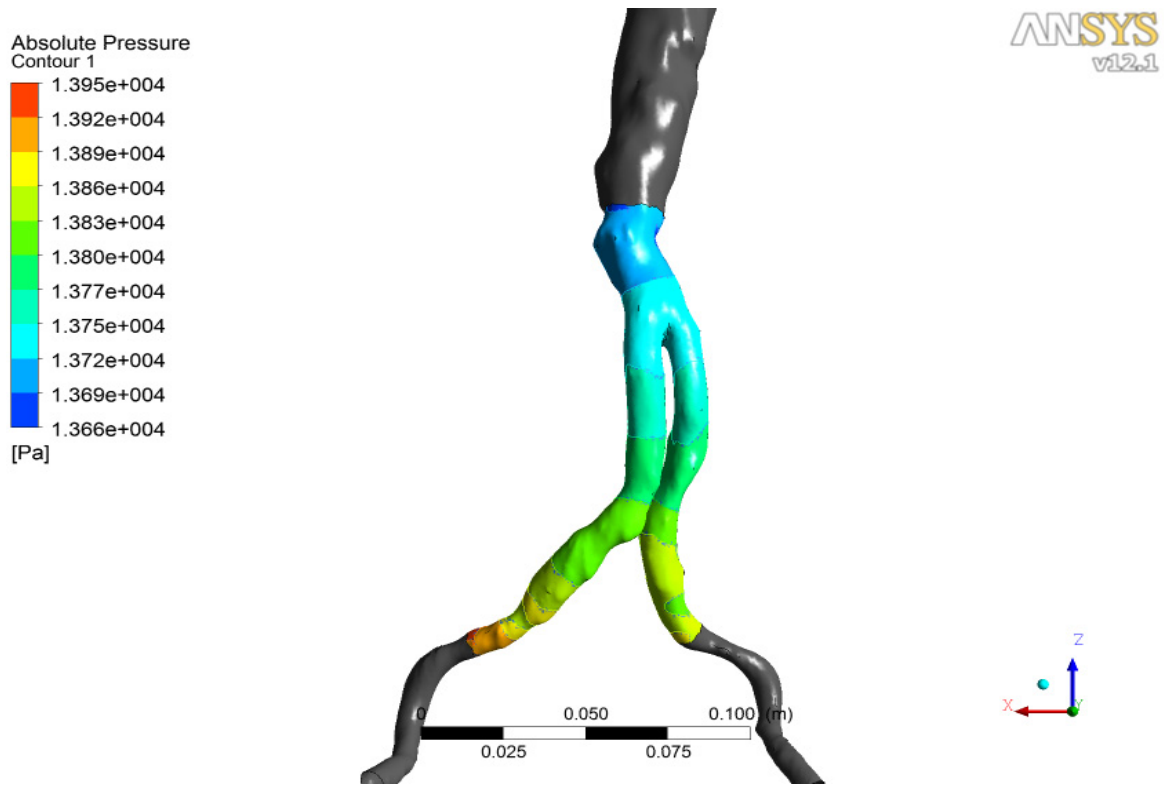


Figure 12. The distribution of pressures across the endograft, as demonstrated for the decelerating systolic phase (t_4).



4.

Figure 13. The distribution of pressures across the endograft, as demonstrated for the end-systolic phase (t_5).

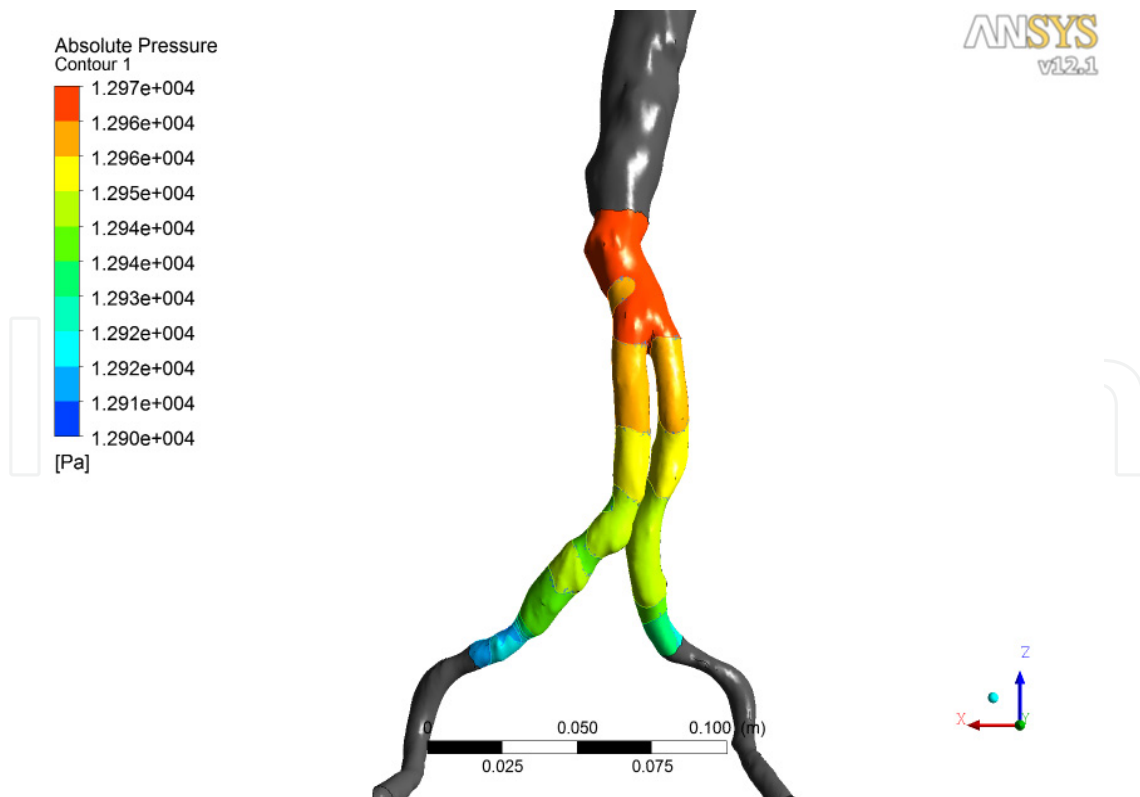


Figure 14. The distribution of pressures across the endograft, as demonstrated for the early diastolic phase (t_6).

Table 1 depicts the minimum and maximum pressure values along the endograft surface, for the different phases of the cardiac cycle (as described above). As depicted in Figures 9-14 and Table 1, there is a similar, homogenous distribution of the pressure values along the different parts of the endograft during the diastolic phase (t_6 and t_1). However, when it comes to the systolic phase (t_2 and t_4), there is a marked linear decrease of the pressure values from the endograft inlet to the iliac limbs (outlet). The greatest pressure value difference is marked in the accelerating systolic phase (t_2). Interestingly, the highest and lowest pressure values are demonstrated in the inlet-main body area and the iliac limbs of the endograft, respectively, during the accelerating and peak systolic phase, whereas this pressure relation is reversed in the decelerating systolic phase (t_4), where the highest values are located distally (outflow). Moreover, there seems to be a narrower range of pressure distribution in the peak systolic phase (t_3). Finally, in the early diastolic phase (t_6) there is again a reverse in the pressure distribution compared to the early systolic phase, with the highest pressure being located in the inflow area of the endograft.

Figures 15-17 demonstrate the vertical velocity patterns and the secondary flow fields in the different parts of the endograft, during the peak systolic and the diastolic phase. The bifurcation of the endograft in two distinct outflow tracts (iliac limbs) causes a disturbance of flow especially in the secondary flow fields and generation of local vortices mainly in the proximal iliac parts (Figure 16), before this marked difference is subsided in the most distal iliac outflow parts (Figure 17). This pattern is also met in the diastolic phase, but with a greater discrepancy being present in this phase (Figures 15-17). In both iliac limbs there was a skewing of the flow towards the inner wall and significant flow separation towards the outer wall.

4. The forces exerted on the endograft surface

The forces applied on the surface of the endograft are demonstrated in Figures 18-20. The forces generated by the pressure are directed mainly vertical to the endograft surface (Figure 18) throughout the cardiac cycle. The tangential forces are mainly caused by the flow of blood and the boundary layer that is formed near the aortic wall, while their direction is depended on the cardiac phase. So, their vector heads forward during the early, peak (Figure 19) and late systolic phase, whereas the direction is reversed during the end systole (Figures 2 and 20) and late diastole. Notably, the values of the tangential forces are lower than the pressure ones by many orders of magnitude. The total sum of the pressure and viscous forces acting on the surface of the graft resolving into the x , y and z components, determines the drag forces that the endograft is subjected to, making it prone to migration.

5. Discussion

(CFD) techniques provide a valuable and reliable tool in the study of the hemodynamic behavior of the cardiovascular system after therapeutic interventions (Frauenfelder, 2006).

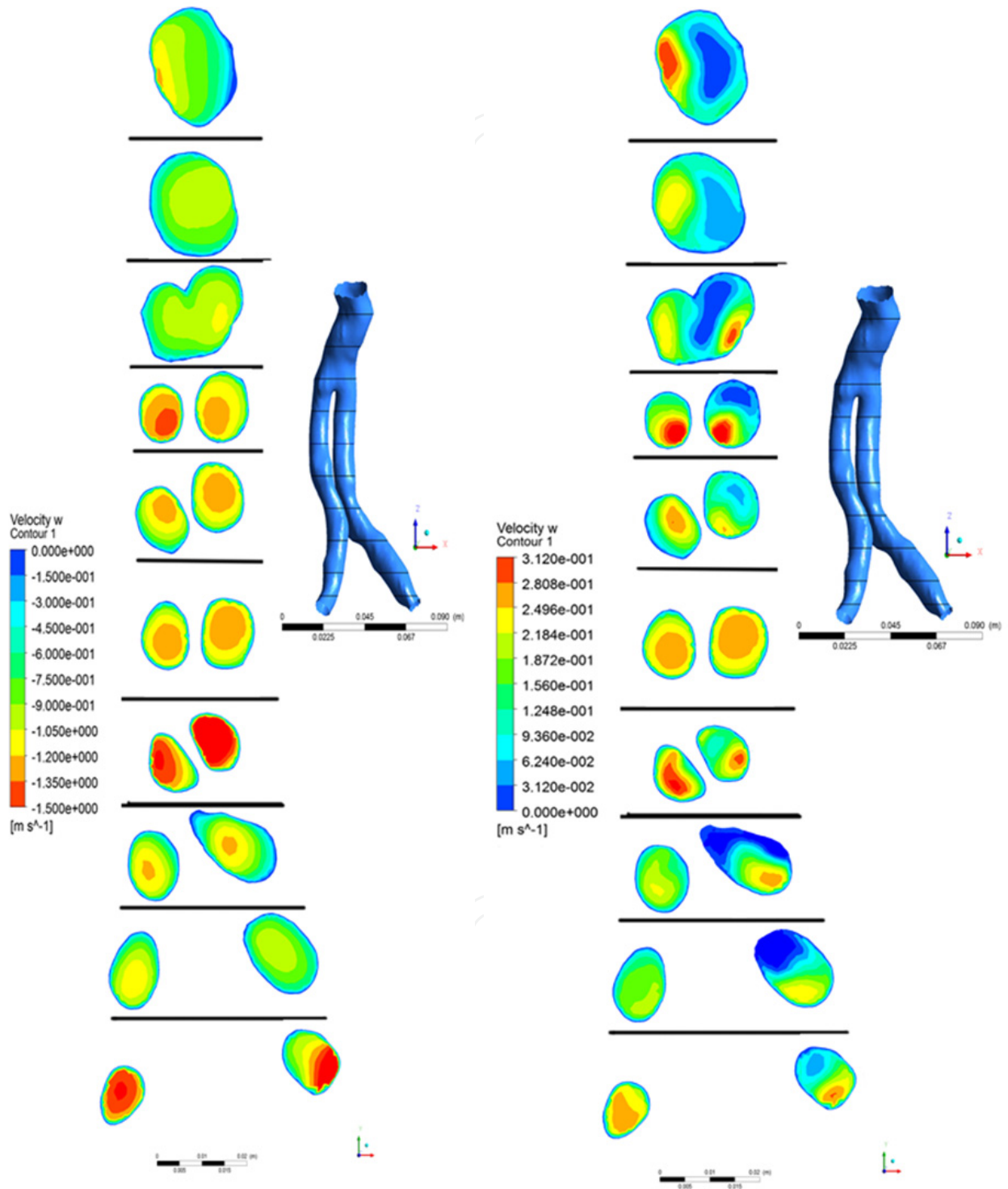


Figure 15. Distribution of velocity values in the transverse axis (-z) along ten cross-section of the endograft, during the peak systolic phase (left panel) and the diastolic phase (right panel).

IntechOpen

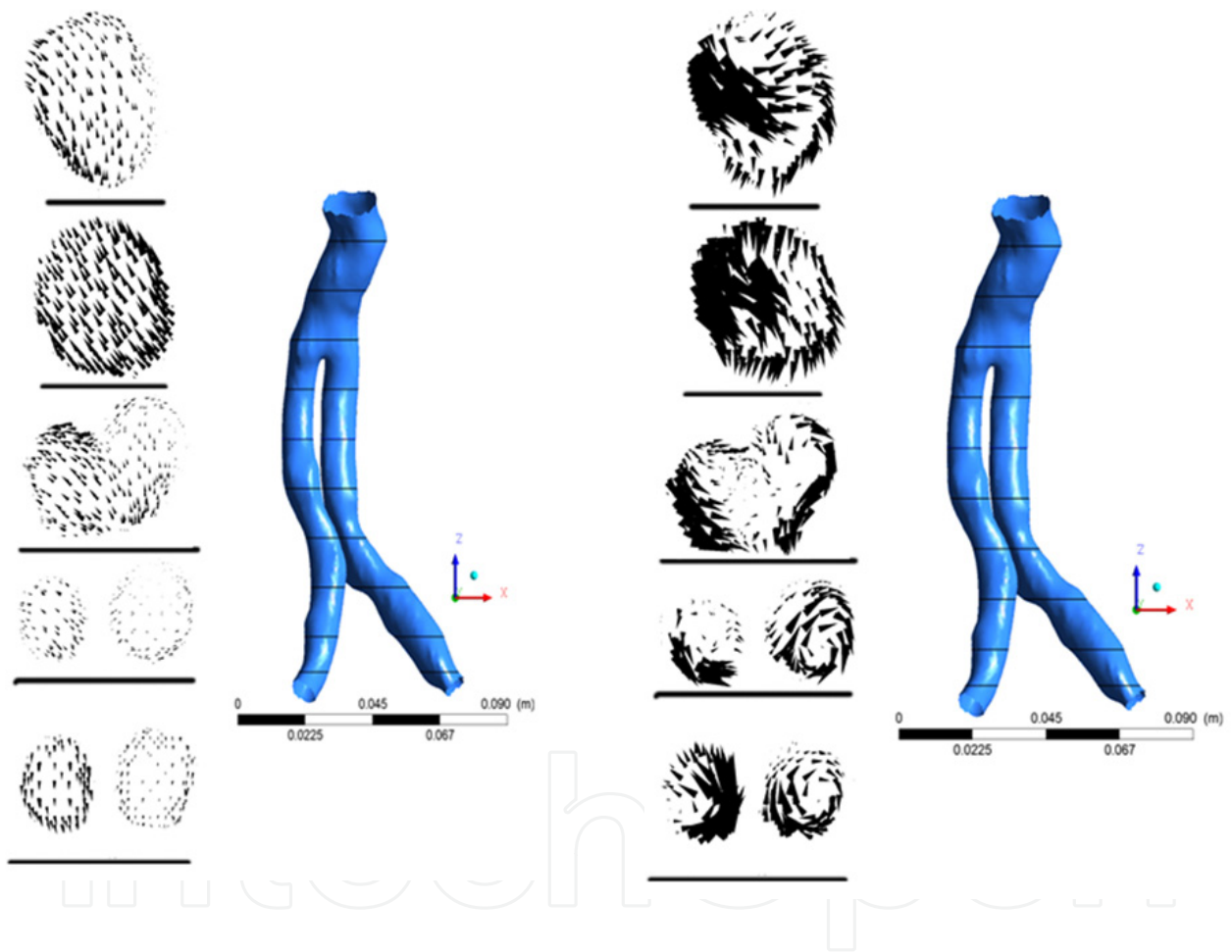


Figure 16. Distribution of velocity profiles in the secondary flow fields along the transverse axis ($-z$) in the 5 cephalad cross-sections (endograft inlet to proximal thirds of the iliac limbs) of the endograft, during the peak systolic (left panel) and the diastolic (right panel) phase.

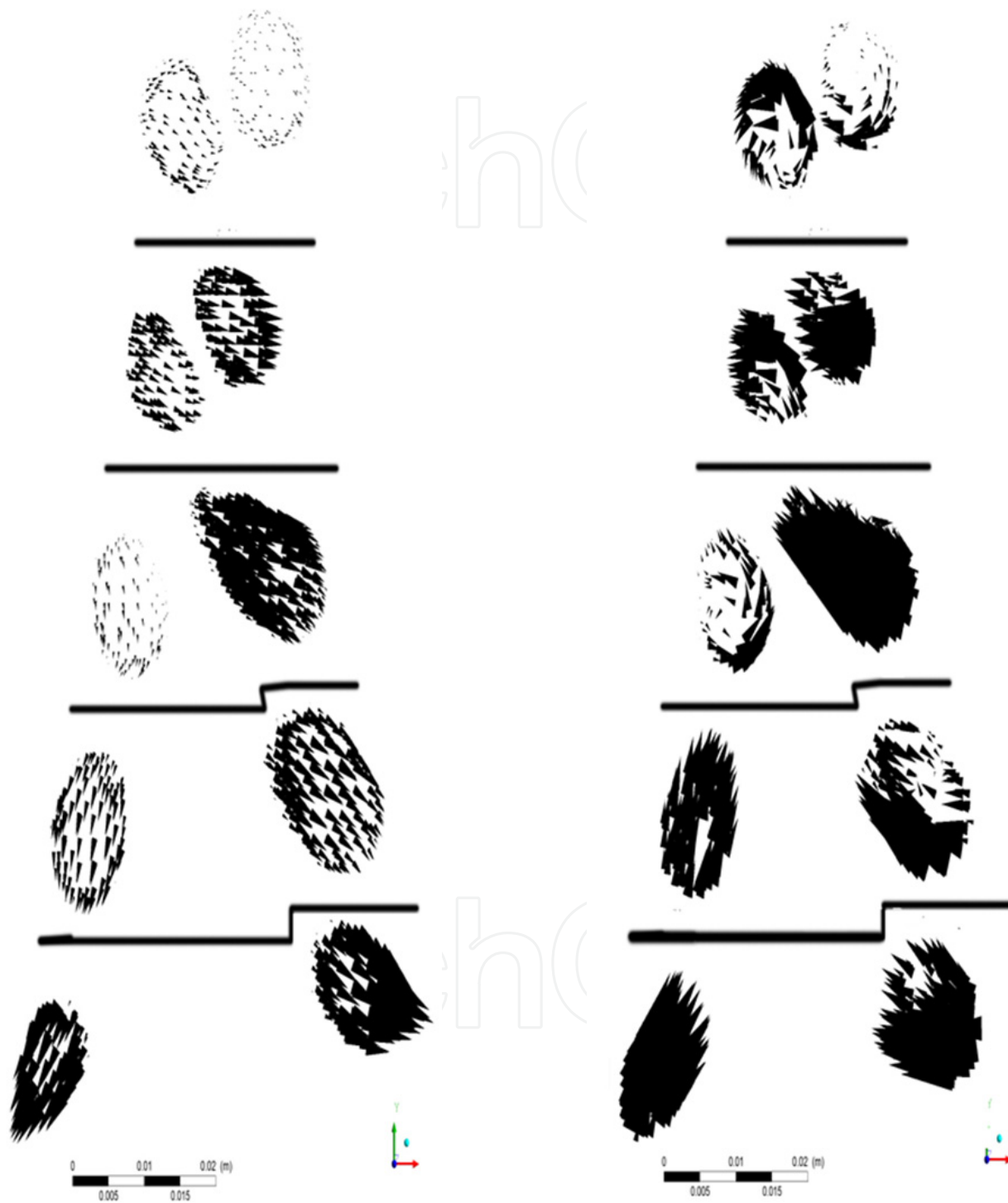


Figure 17. Distribution of velocity profiles in the secondary flow fields along the transverse axis ($-z$) in the 5 caudal cross-sections (proximal to distal thirds of the iliac limbs) of the endograft, during the peak systolic (left panel) and the diastolic (right panel) phase.

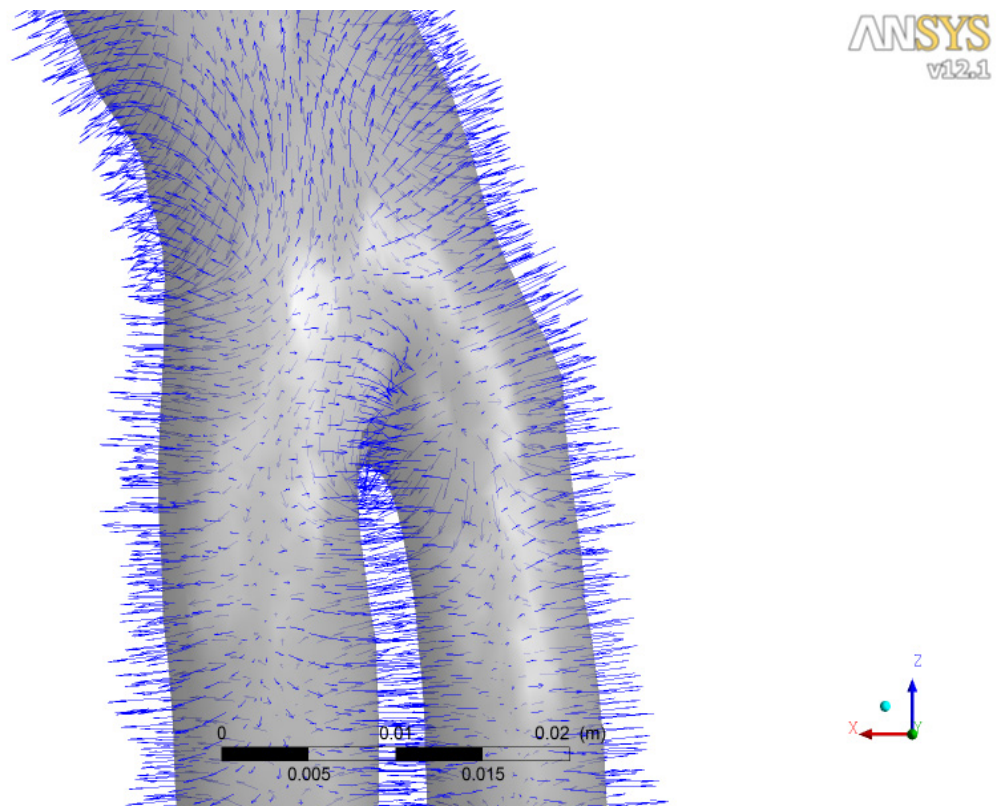


Figure 18. The pressure forces on the endograft bifurcation area (peak systolic phase).

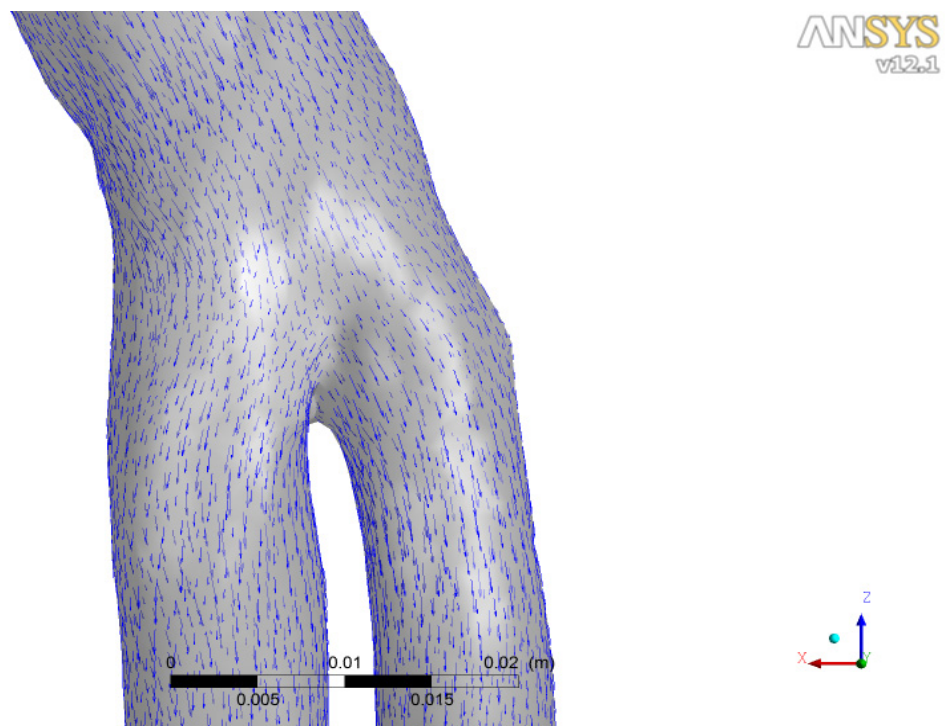


Figure 19. The tangential forces on the endograft bifurcation area (peak systolic phase).

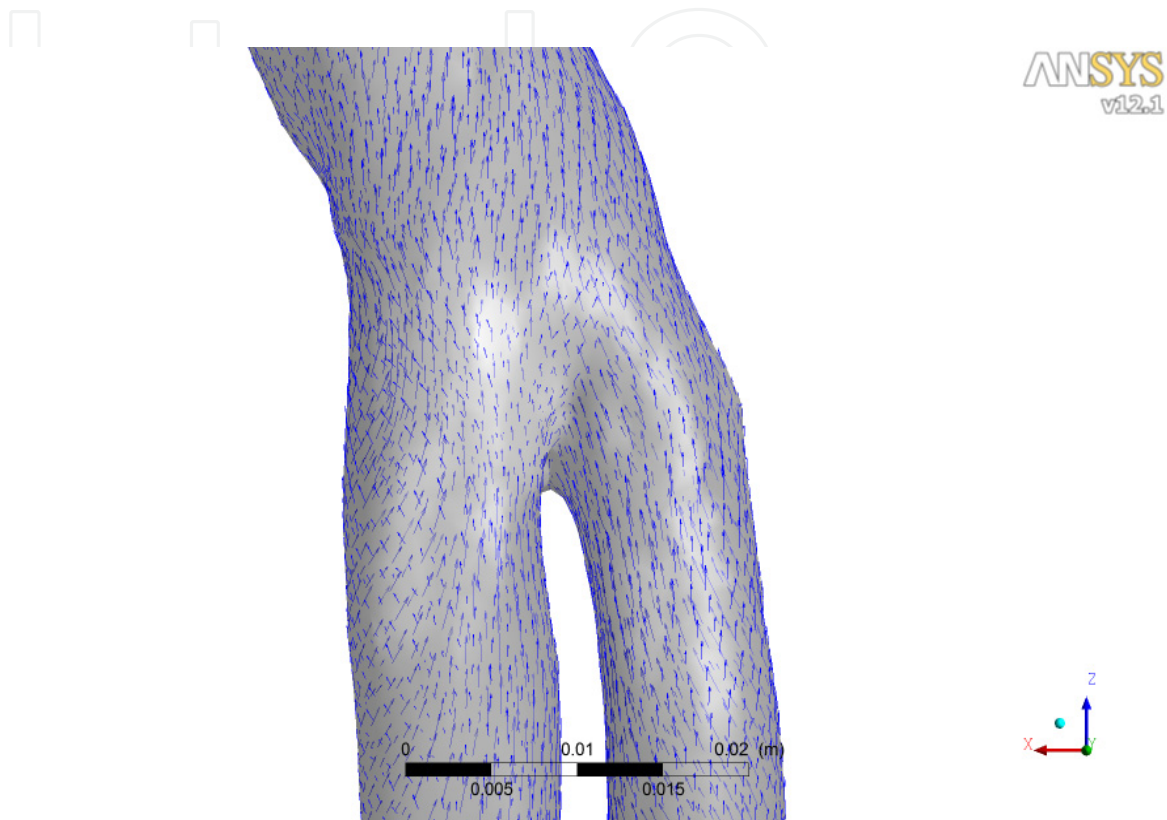


Figure 20. The tangential forces on the endograft bifurcation area during the end systolic phase, t_5).

The insertion of an endograft causes alterations in the hemodynamic environment of the AAA, regarding the pressures and stresses exerted on the AAA sac as well as the flow patterns inside the endograft lumen (Molony et al, 2009). There is a reduction in the intrasac pressure and the stress values on the sac of the stented AAA, leading to sac shrinkage. Chong and How (2004) used flow visualization and laser Doppler anemometry to study in vitro the flow patterns within a stent graft in different phases of the cardiac cycle. According to their study, the main trunk of the endograft is characterized by complex flow patterns with evidence of instability in systolic acceleration phase, developing into a number of vortical structures during systolic deceleration. The flow phenomena in the iliac limbs are strongly influenced by the geometry and the configuration of the limbs (Morris 2006 and Molony, 2008) and any degree of existing constriction caused in the iliac limbs. Basically, the flow in both limbs is triphasic, with a

large retrograde component in end-systole (Chong and How, 2004) and formation of recirculating zones. The profiles are significantly more disturbed in the deceleration phase than at maximum velocity (Chong and How, 2004).

Finally, local geometric factors play a role in the determination of velocity values and flow patterns (recirculating zones, flow separation, skewed flow, vortices and Dean flows) with the out-of-plane endograft geometry determining greatly the outlet flow rates, flow patterns and drag forces (Morris 2006). Extrinsic constriction (due to calcified or stenosed iliac vessels) or excessive kinking in the iliac limbs can lead either to thrombosis of the graft limbs or altered flow patterns that induce excessive disturbances in shear stresses (not shown in our model), leading also to recirculating zones and prolonged transit times of platelets with consequent apposition and formation of thrombus in the endografts. The latter constitutes a rather common incidental finding, occurring more frequently than previously assumed (Wu et al, 2009). Finally, the study and understanding of the hemodynamic alterations and the parameters that influence them, could lead to better designs of endovascular grafts, in order to eliminate the factors that predispose to endograft migration as well as to generation of endoleaks (Figueroa 2009 and 2010, Liffman 2001, Mohan 2002).

6. Conclusion

Aortic endografts are subject to hemodynamic alterations that determine the flow patterns within the different parts of the endografts and influence the values and distribution of pressures and stresses onto their surface during the different phases of the cardiac cycle. Certain geometric factors such as the inlet-to-outlet ratio of the graft as well as the out-of-plane configuration of the main body and iliac limbs have been implicated as major determinants of the aforementioned hemodynamic alterations. Computational simulation techniques can help towards the understanding of these interactions and help us further design better endografts with greater resistance to migration, endoleaks and dislocation of modular stent-grafts, all of which are influenced by the hemodynamic environment that endografts are exposed to.

Author details

Efstratios Georgakarakos, George S. Georgiadis,
Konstantinos C. Kapoulas, Evangelos Nikolopoulos and Miltos Lazarides
*"Democritus" University of Thrace Medical School, Alexandroupolis,
Greece*

Antonios Xenakis
*Fluids Section, School of Mechanical Engineering,
National Technical University of Athens, Athens,
Greece*

7. References

- Georgakarakos E, Georgiadis GS, Ioannou CV, Kapoulas KC, Trellopoulos G, Lazarides M. (2012a). Aneurysm sac shrinkage after endovascular treatment of the aorta: beyond sac pressure and endoleaks. *Vasc Med.*;17:168-73.
- Georgakarakos E, Georgiadis GS, Xenakis A, Kapoulas KC, Lazarides MK, Tsangaris AS, Ioannou CV. (2012b). Application of bioengineering modalities in vascular research: evaluating the clinical gain. *Vasc Endovascular Surg.*;46:101-8.
- Chong CK, How TV, Gilling-Smith GL, Harris PL. (2003). Modeling endoleaks and collateral reperfusion following endovascular AAA exclusion. *J Endovasc Ther.*;10:424-32.
- Chong CK, How TV. (2004). Flow patterns in an endovascular stent-graft for abdominal aortic aneurysm repair. *J Biomech.*;37:89-97.
- Figueroa CA, Taylor CA, Yeh V, Chiou AJ, Zarins CK. (2009). Effect of curvature on displacement forces acting on aortic endografts: a 3-dimensional computational analysis. *J Endovasc Ther.*;16:284-94.
- Figueroa CA, Taylor CA, Yeh V, Chiou AJ, Gorrepati ML, Zarins CK (2010). Preliminary 3D computational analysis of the relationship between aortic displacement force and direction of endograft movement. *J Vasc Surg.*;51:1488-97.
- Frauenfelder T, Lotfey M, Boehm T, Wildermuth S. (2006). Computational fluid dynamics: hemodynamic changes in abdominal aortic aneurysm after stent-graft implantation. *Cardiovasc Intervent Radiol.*;29:613-23.
- Li Z, Kleinstreuer C, Farber M. (2005). Computational analysis of biomechanical contributors to possible endovascular graft failure. *Biomech Model Mechanobiol.*;4:221-34.
- Liffman K, Lawrence-Brown MM, Semmens JB, Bui A, Rudman M, Hartley DE. (2001). Analytical modeling and numerical simulation of forces in an endoluminal graft. *J Endovasc Ther.*;8:358-71.
- Mohan IV, Harris PL, Van Marrewijk CJ, Laheij RJ, How TV. (2002). Factors and forces influencing stent-graft migration after endovascular aortic aneurysm repair. *J Endovasc Ther.*;9:748-55
- Molony DS, Callanan A, Morris LG, Doyle BJ, Walsh MT, McGloughlin TM. (2008). Geometrical enhancements for abdominal aortic stent-grafts. *J Endovasc Ther.*;15:518-29.
- Molony DS, Callanan A, Kavanagh EG, Walsh MT, McGloughlin TM. (2009). Fluid-structure interaction of a patient-specific abdominal aortic aneurysm treated with an endovascular stent-graft. *Biomed Eng Online.*6;8:24.
- Morris L, Delassus P, Grace P, Wallis F, Walsh M, McGloughlin T. (2006). Effects of flat, parabolic and realistic steady flow inlet profiles on idealised and realistic stent graft fits through Abdominal Aortic Aneurysms (AAA). *Med Eng Phys.*;28:19-26.

Olufsen MS, Peskin CS, Kim WY, Pedersen EM, Nadim A, Larsen J. (2000). Numerical simulation and experimental validation of blood flow in arteries with structured-tree outflow conditions. *Ann Biomed Eng.*; 28:1281-99.

Wu IH, Liang PC, Huang SC, Chi NS, Lin FY, Wang SS. (2009). The significance of endograft geometry on the incidence of intraprosthetic thrombus deposits after abdominal endovascular grafting. *Eur J Vasc Endovasc Surg.*;38:741-7.

IntechOpen

IntechOpen